Molecular Physics, Vol. 104, Nos. 22–24, 20 November–20 December 2006, 3619–3626

Vapor–liquid equilibria of water from first principles: comparison of density functionals and basis sets

M. J. MCGRATH†, J. I. SIEPMANN*†, I.-F. W. KUO‡ and C. J. MUNDY‡

†Departments of Chemistry and of Chemical Engineering and Material Science, University of Minnesota, 207 Pleasant St. SE, Minneapolis, Minnesota 55455, USA

‡Chemistry and Materials Science Directorate, Lawrence Livermore National Laboratory, Livermore, CA 94550, USA

(*Received 5 August 2006; in final form 15 September 2006*)

Gibbs ensemble Monte Carlo simulations were run with an efficient mixed-basis electronic structure method to explore the phase equilibria of water from first principles using Kohn–Sham density functional theory. The Perdew–Burke–Ernzerhof exchange/correlation density functional gives a higher critical temperature (700 K) and boiling point (480 K) than experiment, although good agreement is found for the saturated liquid densities. A systematic increase in the size of the basis set for the Becke–Lee–Yang–Parr exchange/correlation density functional from a double-ζ to quadruple-ζ split valence leads to further deviations from experiment on the saturated liquid and vapor densities, while the intermediate basis set gives the best results for the heat of vaporization at $T = 423$ K. Analysis of the liquid structure for all simulations shows changes that can partially be explained by the different densities at a given temperature, and both density functionals show a similar temperature dependence of the liquid structure.

Keywords: Monte Carlo; Density functional theory; Phase equilibria; Water

1. Introduction

The prevalence of water on Earth dictates its important role in biological and terrestrial systems. Soon after the advent of molecular simulation [1, 2], researchers turned their attention to this common, yet mysterious, liquid [3, 4]. Despite significant advances in knowledge since then, a complete understanding of water remains elusive due to its complicated electronic structure (which leads to phenomena such as extensive hydrogen bonding networks and self-dissociation in the liquid phase). This has made elucidating water a grand challenge for liquid state theory and molecular simulation [5–7]. The phase diagram plays an important role in understanding water, as performing liquid simulations for a model which does not have a stable liquid phase at that state point undermines the credibility of the results.

Empirical models of water have been used to compute the vapor–liquid coexistence curve [8] and the complete phase diagram [9], and have the advantage of being relatively inexpensive to use. However, these models lack the flexibility to be applicable in a wide range of environments and state points where the electronic structure of the molecule can fluctuate widely. This is due in part to the need to parameterize them against a specific data set, and in part because many models lack the ability to respond to the local environment (the exception being polarizable models). Choices must also be made on where to locate the interaction sites on a molecule, and these choices may not be universally applicable.

The combination of molecular dynamics (MD) and Kohn–Sham density functional theory by Car and Parrinello (CP) in 1985 [10] provided a method to perform molecular simulations from first principles. In theory, this provides a completely transferable and robust model, although in practice some approximations are still necessary. Shortly after the introduction of the CP method, it was applied to liquid water [11]. This has been followed by further investigations into the mechanical properties of the neat liquid [12–19], supercritical fluid [20–22], solutions [23, 24], the air–water interface [25], and the neat liquid under extreme conditions [26, 27]. Explorations of the thermodynamic properties of water from first principles

*Corresponding author. Email: siepmann@chem.umn.edu

Molecular Physics
ISSN 0026–8976 print/ISSN 1362–3028 online
http://www.tandf.co.uk/journals
DOI: 10.1080/00268970601014781

are considerably fewer due to the added expense of requiring an ensemble average, although some studies have been successfully carried out [28–30]. This work will extend the first-principles simulation study reported in [29] to further determine the effect of first-principles simulation parameters (specifically the exchange/correlation density functional and the Gaussian-type basis set) on the phase equilibrium of water by using Monte Carlo (MC) simulations.

2. Computational details

This study employs the Gibbs ensemble Monte Carlo (GEMC) algorithm [31, 32] to explore the vapor–liquid phase equilibrium properties of water. The energy calculations were performed using the efficient Quickstep routines [33] of the publicly available CP2K package (http://cp2k.berlios.de). These routines use a mixed-basis approach to solving the self-consistent Kohn–Sham equations of density functional theory [34]; atom-centered Gaussian-type orbital functions are used to expand the Kohn–Sham orbitals while plane waves represent the electronic charge density [35]. The Gibbs ensemble algorithm employs two simulation boxes in thermodynamic contact to reproduce bulk phases with no explicit interface. Five distinct move types are used to sample phase space. The first three (molecular translations, rigid-body rotations around the center of mass, and conformational changes in the form of bond stretching and bending) thermally equilibrate the system and are performed on the boxes independently. Volume exchanges between the two boxes achieve mechanical equilibrium, while swapping molecules between the boxes equalizes the chemical potential between the phases. In order to increase efficiency, pre-biasing with an inexpensive potential [36, 37] was done with all three intra-box moves, using a sequence of four to eight moves. Additionally, configurational-bias MC (CBMC) was combined with the inter-box swap move and an inexpensive potential to increase the move acceptance rate [38–40]. Optimal efficiency for the CBMC swap moves was obtained with 640 attempted classical swap moves per Quickstep calculation. The classical potential used for both the biasing of the intra-box and swap moves was fit to the forces obtained from *ab initio* MD simulations [41]. The details of the CP2K implementation of the Monte Carlo routines in both the canonical and Gibbs ensemble are given elsewhere [18, 29, 30].

Two very common exchange/correlation functional combinations used for first-principles molecular simulations are the Becke–Lee–Yang–Parr (BLYP) [42, 43] and Perdew–Burke–Ernzerhof (PBE) [44] functionals. The BLYP functional has been used in previous Monte Carlo simulations in the Gibbs ensemble with a triple-ζ basis set with two sets of *p*-type or *d*-type polarization functions (TZV2P) [29]. In order to provide a more complete view of the accuracy of density functional theory for predicting phase equilibria, two tests were performed here. The first test consisted of GEMC simulations using the PBE density functional with the TZV2P basis set to explore the density functional dependence on the coexistence properties of water. Temperatures of 323, 423, and 523 K were initially used for this test so comparisons to previous studies could be made. However, the 323 K simulation was later stopped because very few swap moves were accepted. Furthermore, even at 523 K the vapor density remained rather low. Consequently, an additional run at 623 K was begun. Several groups have demonstrated that the TZV2P basis set is appropriate for calculations involving generalized gradient approximation (GGA) functionals [33, 45], and therefore the BLYP density functional was combined with double zeta and quadruple zeta basis sets with one and three sets of polarizing functions, respectively (DZVP and QZV3P), in order to provide a systematic examination of basis set dependence. The cost of using the QZV3P basis set is significantly higher than the TZV2P basis set, and therefore the decision was made to only perform the basis set tests at a single temperature (423 K).

All simulations were carried out for systems containing a total of 64 molecules, a system size shown previously to be sufficient as not to show significant finite-size effects [29]. The initial configurations for all runs were taken from the final configuration of the BLYP simulations with the TZV2P basis set at the same temperature [29] and setting the vapor box to be the same size as the liquid box. The initial configuration for 623 K with PBE was the final configuration for BLYP-TZV2P scaled to the experimental liquid density and equilibrated for several picoseconds with a Born–Oppenheimer MD run in the canonical ensemble using CP2K/Quickstep to remove memory of the previous density. A plane-wave cutoff of 1200 Ry for the electronic density was used for all the simulations as this cutoff was shown to be necessary to prevent artifacts in moves that change the volume of a simulation box (and, consequently, the number of grid points used for the energy evaluation) [19]. In accordance with previous works, the norm-conserving pseudopotentials of Goedecker, Teter, and Hutter (GTH) [46, 47] were used to mimic core electrons.

It should be noted that both the nuclei and intramolecular vibrations are treated classically in these simulations. Two studies have previously shown

that water requires a discretization of $\mathcal{O}(10^2)$ in order to converge path integral simulations [48, 49]. Given the current expense of these simulations, this simply is not practical. The coexistence properties of H_2O, D_2O, and T_2O also vary by small amounts relative to the statistical error bars obtained from first-principles Monte Carlo simulations (the respective boiling temperatures are different by less than 1%), and therefore it is unlikely that any differences would be noticed here. The reasons for treating the vibrations classically are somewhat more involved, and the curious reader is referred to [29] for a complete discussion.

Error bars are shown on all graphs where they are larger than the symbol. The computational expense involved in these simulations precludes performing independent simulations and determining the standard deviation of the results, and the runs are too short to separate into multiple parts and do the same analysis. Consequently, errors are estimated by finding the full width at half maximum of the distribution of any given quantity. This provides a measure of the fluctuations that the system undergoes, as well as having the property of remaining approximately constant once a distribution has been adequately sampled.

3. Results and discussion

3.1. *Phase diagram*

3.1.1. Density functional dependence. Figure 1 shows the computed vapor–liquid coexistence densities for all the simulations performed in this work (separated into functional and basis set groups), as well as experimental reference data [50] and the results from previous simulations using the BLYP density functional and the standard triple-ζ basis set [29]. One very noticeable feature of this graph is how well the PBE-GTH-TZV2P-1200 representation appears to reproduce the saturated liquid density of water across the range of 423–623 K, with relatively small error bars almost encompassing the experimental densities. However, a higher critical temperature than experiment (700 K vs. 647 K) is predicted because of the significant underestimation of the saturated vapor densities. The Clausius–Clapeyron plot of the saturated vapor pressures (figure 2) is also affected by the underestimated vapor densities, resulting in a predicted boiling temperature of 480 K for PBE-GTH-TZV2P-1200. The vapor pressures were computed using the ideal gas law. Given the low vapor densities between 423 and 623 K and the linear form of the resulting Clausius–Clapeyron plot shown in figure 2, this appears to be a valid approximation. The temperature dependence of the heat of vaporization is shown in figure 3 and the results are consistently higher than experiment for PBE-GTH-TZV2P-1200, which agrees with the picture presented by figures 1 and 2 that this representation of water is overbound with respect to experiment.

A study has recently appeared that examined the accuracy of a wide range of Kohn–Sham density functionals on predicting the energetics of small water clusters and reports modifications to existing functionals

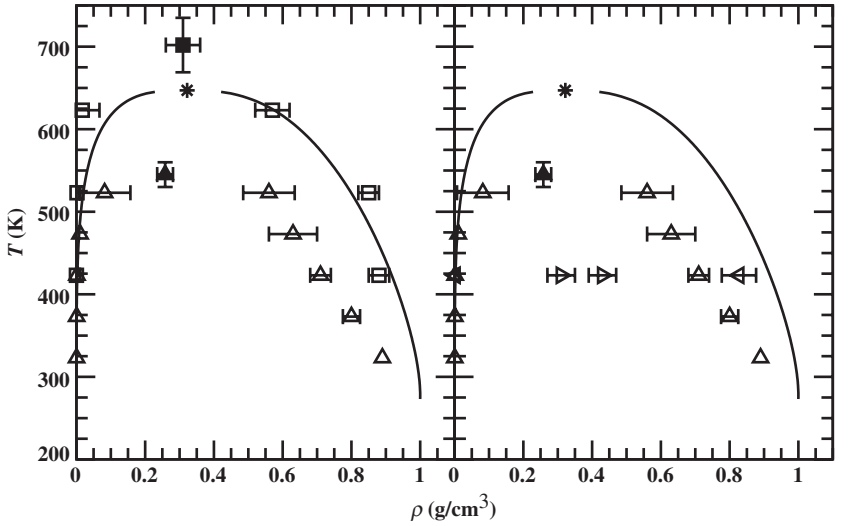

Figure 1. The computed vapor–liquid coexistence curves for water shown as a function of Kohn–Sham density functional (left panel) and basis set (right panel). Solid lines and stars represent the experimental results [50]. Filled symbols depict critical temperatures calculated by combining the law of rectilinear diameters and the saturated density scaling law. Results are shown for the BLYP density functional with double (triangle left), triple (triangle up), and quadruple (triangle right) zeta basis sets, and the PBE density functional with a triple zeta basis set (square). Results for BLYP with a triple zeta basis set are taken from [29]. Error bars are explained in the text.

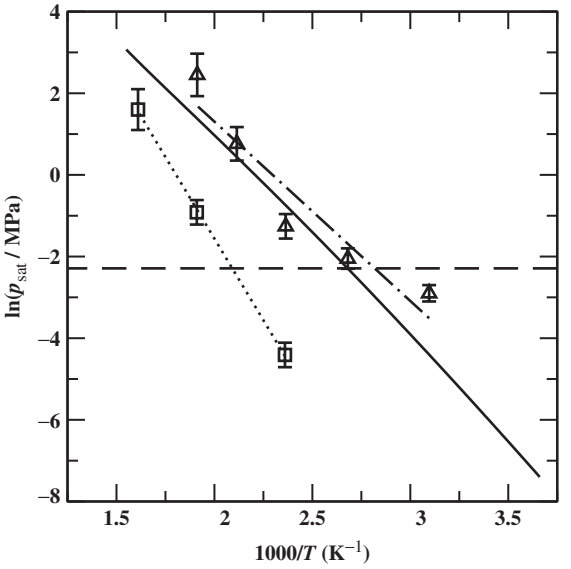

Figure 2. Clausius–Clapeyron plots for water using various Kohn–Sham density functionals. The symbols are the same as figure 1. Unweighted linear fits are shown for BLYP (dash-dotted) and PBE (dotted) functionals as guides for the eye. A line corresponding to one atmosphere pressure (dashed) is shown as an aide in determining boiling temperatures. Results are shown only for functional/basis set combinations for which a unique line can be determined.

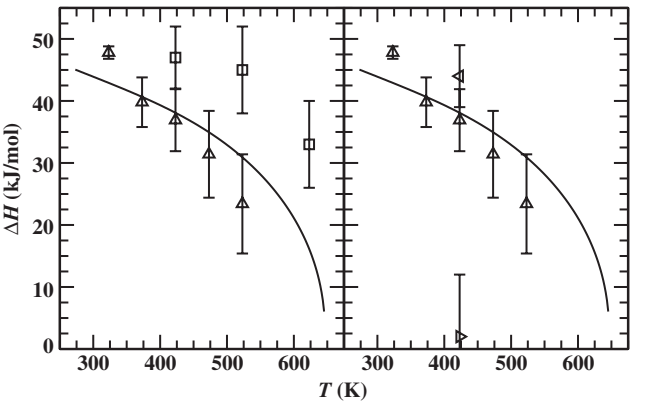

Figure 3. Heats of vaporization as a function of temperature for water with different Kohn–Sham density functionals (left panel) and basis sets (right panel). The symbols are the same as figure 1.

to improve them [51]. The basis set used in the calculations was MG3S [52], which is a triple-ζ basis set with polarization functions, which is different from the TZV2P basis set used here for its inclusion of diffuse functions. There is no reason why a meaningful comparison cannot be drawn between the results obtained in [51] and those reported here, despite the difference in basis set. This study showed that PBE yields overbinding for the series of dimers and trimers tested, while BLYP yields underbinding for the same structures. The magnitude of the error for BLYP is also significantly larger than for PBE (by a factor of 2). These results qualitatively and quantitatively agree with the critical temperatures obtained from this study (the critical temperature for PBE-GTH-TZV2P-1200 is about 50 K higher than experiment, while the BLYP-GTH-TZV2P-1200 model underpredicts it by about 100 K), although the quantitative agreement is probably fortuitous.

3.1.2. Basis set dependence. Figures 1 and 3 show the computed coexistence densities and heats of vaporization for the BLYP-GTH-DZVP-1200, BLYP-GTH-TZV2P-1200, and BLYP-GTH-QZV3P-1200 simulations performed here. The saturated vapor pressures are not shown on the Clausius–Clapeyron plot as these simulations were done only at one temperature, and therefore an accurate estimation of the boiling point cannot be made. Several observations can be made about these simulations. The first is that the more complete QZV3P basis set actually leads to larger deviations from experiment for the BLYP density functional. It also appears that the satisfactory agreement in the heat of vaporization for the TZV2P basis set reported in [29] is due to a cancelation of errors, as the DZVP basis set and QZV3P basis set over and under estimate this quantity, respectively. Several groups have recently explored the basis set dependence of small cluster energetics [51, 53, 54] and determined that a double-ζ basis set is the most accurate for BLYP while PBE does best with a much larger basis; these results appear to be supported here, although more extensive tests are needed to confirm this.

One of the drawbacks of using atom-centered basis sets is the introduction of basis set superposition error (BSSE). BSSE adds cohesive energy to the system through the 'borrowing' of basis functions from neighboring molecules, thus artificially increasing the size of the basis set. This error increases as the size of the basis set decreases, so one would expect that the DZVP simulations in this work would suffer from the largest error. There exists a variety of methods for removing the BSSE in small clusters, but they grow quickly in complexity and expense with increasing system size until they are impractical for simulations in the liquid phase and even the proper method becomes ambiguous [55, 56].

While the same basis set trend is shown in both figures 1 and 3, the quantitative results are a little harder to explain. Tests on the water dimer show that the BSSE shrinks by about 50% when moving from a DZVP basis set to TZV2P, and again when moving from TZV2P to QZV3P (computed using the counterpoise correction [57]). This means that the absolute error difference is

significantly larger between DVZP and TZV2P than TZV2P and QZV3P. However, the opposite is true for the saturated liquid densities at 423 K, i.e. the result for TZV2P is closer to that for DZVP than that for QZV3P. The likely reason is that use of QZV3P results in a large downward shift of the critical temperature, so that the temperature of 423 K already corresponds to a near-critical temperature where the coexistence curve is rounded. A more complete test would be to compute the full coexistence curves for each basis set and compare the resulting critical temperatures, but due to expense this has not yet been done.

The observed sensitivity of the vapor–liquid coexistence curve is at variance with earlier results in the microcanonical ensemble where changing the size of the basis set for an *ab initio* molecular dynamics simulation of water had negligible effects on structural and transport properties [58]. This again reinforces that simulations in an open ensemble are more sensitive to the simulation parameters and are, therefore, a much better test of the accuracy of a given model [59–61].

3.2. *Structural properties*

The three radial distribution functions (RDFs) for water (between oxygen–oxygen, oxygen–hydrogen, and hydrogen–hydrogen) at $T = 423$ K are shown in figure 4. The most significant feature of this graph is the substantial broadening of the peaks for BLYP-GTH-QZV3P-1200 as compared to the other three runs. The obvious reason for this is seen in figure 1, which contains the liquid densities of each system. BLYP-GTH-QZV3P-1200 appears to be very close to the critical temperature (enough so that the phase identity of the simulation boxes inverted over the course of the simulation), which means the liquid will be near its critical density, which consequently leads to less structure (a result seen in all three panels of figure 4). The other feature that is readily discernible is that the peak locations of PBE-TZV2P-GTH-1200 are shifted to smaller distances, which again is explained by the higher density of this simulation at this temperature. This is most noticeable for the first peak and minimum in the oxygen–hydrogen RDF. It should be noted that the heights of the first peak in the oxygen–oxygen RDF for both BLYP-GTH-TZV2P-1200 and PBE-GTH-TZV2P-1200 are very similar (within about 0.2). The result has been seen before in molecular dynamics simulations at a fixed density [18, 58], but is somewhat more surprising here given the extra degrees of freedom in the system. With the exception of BLYP-GTH-QZV3P-1200, the other three functional/basis set combinations yield a weak second peak at about 5 Å in the oxygen–oxygen RDF, but it remains an open question whether this second peak would still be present for simulations using much larger system sizes.

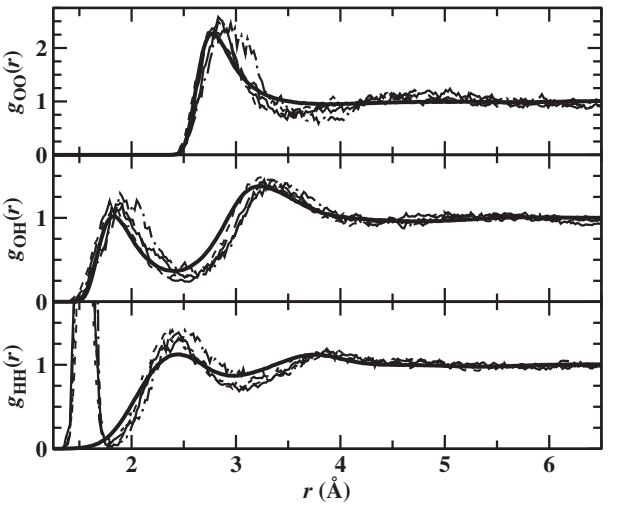

Figure 4. Radial distribution functions for oxygen–oxygen (top), oxygen–hydrogen (middle), and hydrogen–hydrogen (bottom) pairs in water as a function of Kohn–Sham density functional and basis set. All data shown is for the saturated liquid phase at $T = 423$ K. The simulations are: BLYP with the TZV2P basis set (solid), PBE with the TZV2P basis set (dotted), BLYP with the DZVP basis set (dashed), and BLYP with the QZV3P basis set (dash-dotted). Results for the polarizable TIP4P-pol2 model [64] are shown as thick solid lines. A bin size of 0.02 Å was used for all three graphs.

The structure of liquid water at elevated temperatures and ambient or higher pressure has been probed by X-ray and neutron diffraction experiments [13, 62, 63]. However, transforming the raw scattering data into separate atom–atom radial distribution functions is not a straightforward procedure and involves some approximations [13, 63]. Neutron data were obtained by Soper *et al.* [62] for liquid water at $T = 423$ K and $\rho = 0.92\,\mathrm{g\,cm^{-3}}$, i.e. close to the experimental saturated liquid density at 423 K but somewhat higher than the coexistence densities calculated here for the various functional and basis set combinations. Soper and co-workers obtained the individual atom–atom RDFs via empirical potential structure refinement (EPSR) simulations fit to neutron diffraction data and reported two different sets of RDFs. The more recent analysis [63] gives a height of about 2.7 for the first peak and a noticeable peak for the second solvation shell in the oxygen–oxygen RDF. In contrast, a height of 1.9 was originally reported for the same dataset with a significantly less noticeable second solvation shell [62]). Accurate X-ray scattering experiments were recently reported for liquid water at ambient pressure and a temperature of 348 K [13]. The X-ray scattering intensities over a substantial temperature range are very well

reproduced by the polarizable TIP4P-pol2 model [64] and the real-space RDF for this model gives a first peak height of about 2.6 and a small peak for the second solvation shell at 350 K. For comparison, the three RDFs computed for the TIP4P-pol2 model using $N = 500$ at 423 K and the experimental saturated liquid density are shown in figure 4. At this state point, the oxygen–oxygen RDF for the TIP4P-pol2 model shows a first peak height of about 2.2 and no discernable peak for the second solvation shell. Previous simulations employing empirical interaction potentials have resulted in a range of first peak heights in the oxygen–oxygen RDF of 2.1–2.5 and only one out of four models yielded a significant second peak at about 5 Å [65]. Given the large uncertainties of the experimental RDFs (estimated to account for a 10% variation in the RDFs [63]) and the significant statistical uncertainties encountered in first-principles simulations (relatively short simulation lengths for small systems), it is apparent that RDFs are not a good tool to discriminate between the different functional/basis set combinations used here.

The structure of the first solvation shell of water has been debated for several years [66, 67]. While the temperatures in those studies are significantly lower than here, the analysis methods outlined are useful to explore the symmetry of the local environment in these simulations. One would expect that, in a perfectly tetrahedral crystal (that is, when the four nearest neighbors of a given water molecule sit on the vertices of a tetrahedron centered on that molecule), the average difference of the separation of the two nearest oxygen atoms and the next two nearest oxygen atoms from the central oxygen is zero. It was shown in a previous report [29] that not only is this quantity non-zero for BLYP-GTH-TZV2P-1200 but the difference increases as a function of temperature, suggesting an increase in the asymmetry of the local water environment. An identical trend is seen for PBE-GTH-TZV2P-1200 in this work, as shown in the top panel of figure 5, indicating that this pattern is not determined by the choice of functional used in the calculation.

The lower panel in figure 5 provides information on the hydrogen bonding occurring in the PBE and BLYP simulations with an identical basis set. A population analysis of the average hydrogen bond donor status (non-donor, single donor, and double donor) as a function of temperature and Kohn–Sham density functional is shown here, using the angular-distance criterion proposed in [66]. While the fraction of single donors still does not climb to the 0.80 seen in [66], the results of all donor fractions follow the same trend for PBE as BLYP. This trend is not surprising, as the saturated liquid density of the systems also decreases with temperature. As the average distance between

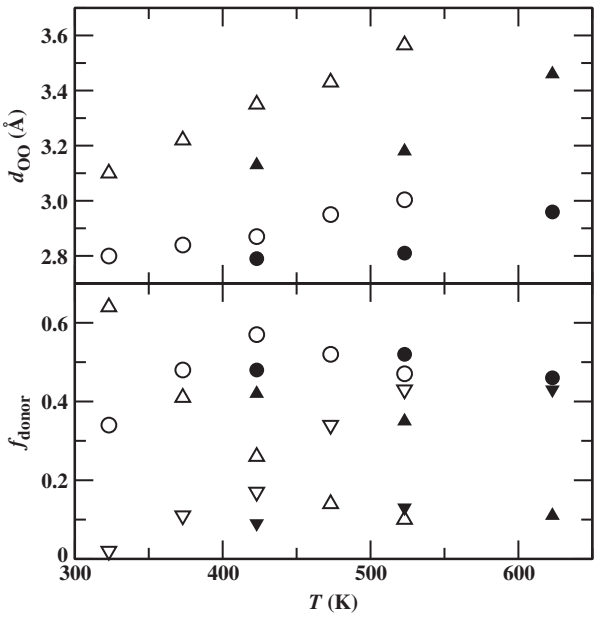

Figure 5. (Top) Temperature dependence of the oxygen–oxygen distances to the two nearest (circle) and two next-nearest (triangle up) molecules in the coordination shell for the saturated liquid phase. (Bottom) Temperature dependence of the faction of double-donor (triangle up), single-donor (circle), and non-donor (triangle down) configurations. Results for BLYP are taken from [29] and shown with open symbols, while those for PBE are shown with filled symbols. Error bars are not shown for clarity, but the typical errors are ±0.15 and ±0.25 Å for the shorter and longer distances, respectively, in the top panel and ±0.05 for the bottom panel.

molecules increases, any bonding criterion that employs a distance cutoff will label fewer pairs as 'hydrogen bonds', consequently reassigning double donors to single donors and single donors to non-donors.

One final measure of structure in a liquid simulation is the tetrahedral order parameter, q, as renormalized by Errington and Debenedetti [68]. In a crystal where every oxygen is the center of a tetrahedron, the value of q will be 1, where an ideal gas will have a value of 0. The values of q for all four systems are shown in figure 6, and the values appear to be linearly related to the liquid density and tending towards disorder as the temperature increases. This graph also suggests that the value of q near the critical temperature will be around 0.3, regardless of the functional or basis set.

The relationship between the four measures of order depicted in this work (RDF, oxygen–oxygen asymmetry, hydrogen bond populations, and q) is obfuscating. In terms of reduced temperature (T/T_c), 323 K is approximately the same for BLYP-GTH-TZV2P-1200 as 423 K is for PBE-GTH-TZV2P. This is supported by the oxygen–oxygen asymmetry and saturated liquid density, but none of the other three measures of structure.

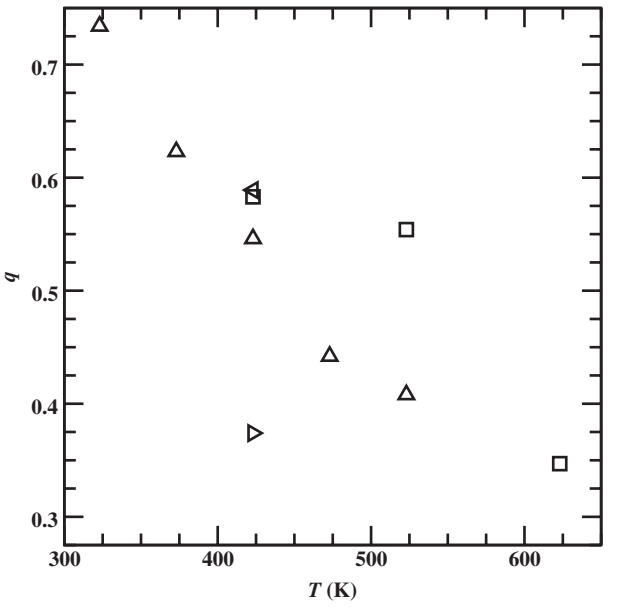

Figure 6. Tetrahedral order parameter [68] as a function of temperature and Kohn–Sham density functional. Symbols are the same as figure 1. Error bars are not shown for clarity, but the typical errors are ±0.25 for q.

Instead, BLYP at 323 K has more double donors, a higher peak in the oxygen–oxygen RDF [29], and a larger value of the tetrahedral order parameter. This indicates that intermolecular structure is not the only factor that determines the coexistence properties of a system.

4. Conclusion

Gibbs ensemble Monte Carlo simulations from first principles were used to examine the effect of the Kohn–Sham exchange/correlation density functional and Gaussian-type basis set on the vapor–liquid equilibrium of water. The results show that the PBE-GTH-TZV2P-1200 representation yields a higher critical temperature, a higher boiling point, higher saturated liquid densities, and higher heats of vaporization than BLYP-GTH-TZV2P-1200, and although the saturated liquid densities of PBE agree fairly well with experiment over the temperature range studied, its saturated vapor pressures are too low and heats of vaporization are too high. Using the BLYP density functional and systematically changing the basis set at a single temperature results in a more complete basis set producing increased deviations from experiment.

This work confirms the belief that phase equilibria are extremely sensitive to first-principles parameters of the system, something that has been known for empirical potentials for some time. Future work will continue the tests performed here for the system's plane wave cutoff and choice of pseudopotential, as well as examining functionals parameterized to reproduce small water cluster energetics accurately and testing standard functionals on different molecular fluids. This knowledge will enable one to select an appropriate density functional for the system and property of interest while also providing a guide for developing the next generation of Kohn–Sham exchange/correlation density functionals.

Acknowledgements

We thank Larry Fried and Charlie Westbrook for their ongoing support of this work. We also thank Juerg Hutter, Joost VandeVondele, Matthias Krack, Erin Dahlke, and Bin Chen for many stimulating discussions. Financial support from the National Science Foundation (CTS-0553911), a 3M Foundation Graduate Fellowship (M.J.M.), and a Department of Energy Computational Science Graduate Fellowship (M.J.M.) are gratefully acknowledged. Part of this work was performed under the auspices of the U.S. Department of Energy by the University of California Lawrence Livermore National Laboratory (LLNL) under contract No. W-7405-Eng-48. Computer resources were provided by Livermore Computing and the Minnesota Supercomputing Institute.

References

[1] N. Metropolis, A. W. Rosenbluth, M. N. Rosenbluth, A. H. Teller and E. Teller, J. Chem. Phys. **21,** 1087 (1953).
[2] B. J. Alder and T. E. Wainwright, J. Chem. Phys. **31,** 459 (1959).
[3] J. A. Barker and R. O. Watts, Chem. Phys. Lett. **3,** 144 (1969).
[4] A. Rahman and F. H. Stillinger, J. Chem. Phys. **55,** 3336 (1971).
[5] F. H. Stillinger, Science **209,** 451 (1980).
[6] J. P. Hansen and I. R. McDonald, *Theory of Simple Liquids*, 3rd ed. (Academic Press, New York, 2006).
[7] B. Guillot, J. Molec. Liq. **101,** 219 (2002).
[8] J. J. de Pablo, J. M. Prausnitz, H. J. Strauch and P. T. Cummings, J. Chem. Phys. **93,** 7355 (1990).
[9] E. Sanz, C. Vega, J. L. F. Abascal and L. G. MacDowell, Phys. Rev. Lett. **92,** 255701 (2004).
[10] R. Car and M. Parrinello, Phys. Rev. Lett. **55,** 2471 (1985).
[11] K. Laasonen, M. Sprik, M. Parrinello and R. Car, J. chem. Phys. **99,** 9080 (1993).
[12] P. L. Silvestrelli and M. Parrinello, J. Chem. Phys. **111,** 3572 (1999).
[13] G. Hura, D. Russo, R. M. Glaeser, T. Head-Gordon, M. Krack and M. Parrinello, Phys. Chem. Chem. Phys. **5,** 1981 (2003).
[14] J. C. Grossman, E. Schwegler, E. W. Draeger, F. Gygi and G. Galli, J. Chem. Phys. **120,** 300 (2004).

[15] E. Schwegler, J. C. Grossman, F. Gygi and G. Galli, J. Chem. Phys. **121,** 5400 (2004).
[16] P. H.-L. Sit and N. Marzari, J. Chem. Phys. **122,** 204510 (2005).
[17] M. V. Fernández-Serra and E. Artacho, J. Chem. Phys. **121,** 11136 (2004).
[18] I-F. W. Kuo, C. J. Mundy, M. J. McGrath, J. I. Siepmann, J. VandeVondele, M. Sprik, J. Hutter, B. Chen, M. L. Klein, F. Mohamed, M. Krack and M. Parrinello, J. Phys. Chem. B **108,** 12990 (2004).
[19] M. J. McGrath, J. I. Siepmann, I-F. W. Kuo, C. J. Mundy, J. VandeVondele, J. Hutter, F. Mohamed and M. Krack, ChemPhysChem **6,** 1894 (2005).
[20] E. S. Fois, M. Sprik and M. Parrinello, Chem. Phys. Lett. **223,** 411 (1994).
[21] M. Boero, K. Terakura, T. Ikeshoji, C. C. Liew and M. Parrinello, Phys. Rev. Lett. **85,** 3245 (2000).
[22] M. Boero, K. Terakura, T. Ikeshoji, C. C. Liew and M. Parrinello, J. Chem. Phys. **115,** 2219 (2001).
[23] P. L. Geissler, C. Dellago, D. Chandler, J. Hutter and M. Parrinello, Science **291,** 2121 (2001).
[24] M. E. Tuckerman, D. Marx and M. Parrinello, Nature **417,** 925 (2002).
[25] I-F. W. Kuo and C. J. Mundy, Science **303,** 658 (2004).
[26] C. Cavazzoni, G. L. Chiarotti, S. Scandolo, E. Tosatti, M. Bernasconi and M. Parrinello, Science **283,** 44 (1999).
[27] A. F. Goncharov, N. Goldman, L. E. Fried, J. C. Crowhurst, I-F. W. Kuo, C. J. Mundy and J. M. Zaug, Phys. Rev. Lett. **94,** 125508 (2005).
[28] D. Asthagiri, L. R. Pratt and J. D. Kress, Phys. Rev. E **68,** 041505 (2003).
[29] M. J. McGrath, J. I. Siepmann, I-F. W. Kuo, C. J. Mundy, J. VandeVondele, J. Hutter, F. Mohamed and M. Krack, J. Phys. Chem. A **110,** 640 (2006).
[30] M. J. McGrath, J. I. Siepmann, I-F. W. Kuo, C. J. Mundy, J. VandeVondele, M. Sprik, J. Hutter, F. Mohamed, M. Krack and M. Parrinello, Comput. Phys. Commun. **169,** 289 (2005).
[31] A. Z. Panagiotopoulos, Molec. Phys. **61,** 813 (1987).
[32] A. Z. Panagiotopoulos, N. Quirke, M. Stapleton and D. J. Tildesley, Molec. Phys. **63,** 527 (1988).
[33] J. VandeVondele, M. Krack, F. Mohamed, M. Parrinello, T. Chassaing and J. Hutter, Comput. Phys. Commun. **167,** 103 (2005).
[34] W. Kohn and L. J. Sham, Phys. Rev. **140,** A1133 (1965).
[35] G. Lippert, J. Hutter and M. Parrinello, Molec. Phys. **92,** 477 (1997).
[36] R. Iftimie, D. Salahub, D. Wei and J. Schofield, J. Chem. Phys. **113,** 4852 (2000).
[37] L. D. Gelb, J. chem. Phys. **118,** 7747 (2003).
[38] J. I. Siepmann and D. Frenkel, Molec. Phys. **75,** 59 (1992).
[39] B. Smit, S. Karaborni and J. I. Siepmann, J. Chem. Phys. **102,** 2126 (1995).
[40] T. J. H. Vlugt, M. G. Martin, B. Smit, J. I. Siepmann and R. Krishna, Molec. Phys. **94,** 727 (1998).
[41] S. Izvekov, M. Parrinello, C. J. Burnham and G. A. Voth, J. Chem. Phys. **120,** 10896 (2004).
[42] A. D. Becke, Phys. Rev. A **38,** 3098 (1988).
[43] C. Lee, W. Yang and R. G. Parr, Phys. Rev. B **37,** 785 (1988).
[44] J. P. Perdew, K. Burke and M. Ernzerhof, Phys. Rev. Lett. **77,** 3865 (1996).
[45] A. D. Boese, J. M. L. Martin and N. C. Handy, J. Chem. Phys. **119,** 3005 (2003).
[46] S. Goedecker, M. Teter and J. Hutter, Phys. Rev. B **54,** 1703 (1996).
[47] C. Hartwigsen, S. Goedecker and J. Hutter, Phys. Rev. B **58,** 3641 (1998).
[48] W. Shinoda and M. Shiga, Phys. Rev. E **71,** 041204 (2005).
[49] Y. A. Mantz, B. Chen and G. J. Martyna, Chem. Phys. Lett. **405,** 294 (2005).
[50] NIST Chemistry Webbook (http://webbook.nist.gov).
[51] E. E. Dahlke and D. G. Truhlar, J. Phys. Chem. B **109,** 15677 (2005).
[52] B. J. Lynch, Y. Zhao and D. G. Truhlar, J. Phys. Chem. A **107,** 1384 (2003).
[53] G. I. Csonka, A. Ruzsinszky and J. P. Perdew, J. Phys. Chem. B **109,** 21471 (2005).
[54] E. E. Dahlke and D. G. Truhlar, J. Phys. Chem. B **110,** 10595 (2006).
[55] K. Mierzwicki and Z. Latajka, Chem. Phys. Lett. **380,** 654 (2003).
[56] T. Malaspina, K. Coutinho and S. Canuto, J. Chem. Phys. **117,** 1692 (2002).
[57] S. F. Boys and F. Bernardi, Molec. Phys. **19,** 553 (1970).
[58] J. VandeVondele, F. Mohamed, M. Krack, J. Hutter, M. Sprik and M. Parrinello, J. Chem. Phys. **122,** 014515 (2005).
[59] B. Smit, J. Chem. Phys. **96,** 8639 (1992).
[60] J. I. Siepmann, S. Karaborni and B. Smit, Nature **365,** 330 (1993).
[61] J. I. Siepmann, in *Forum 2000: Fluid Properties for New Technologies*, Connecting Virtual Design with Physical Reality, NIST Special Publication 975, edited by J. C. Rainwater, D. G. Friend, H. H. J. M. Hanley, A. H. Harvey, C. D. Holcomb, A. Laesecke, J. Magee and C. Munzy (NIST, Boulder, 2001), p. 110.
[62] A. K. Soper, F. Bruni and M. A. Ricci, J. Chem. Phys. **106,** 247 (1997).
[63] A. K. Soper, Chem. Phys. **258,** 121 (2000).
[64] B. Chen, J. Xing and J. I. Siepmann, J. Phys. Chem. B **104,** 2391 (2000).
[65] A. A. Chialvo, E. Yezdimer, T. Driesner, P. T. Cummings and J. M. Simonson, Chem. Phys. **258,** 109 (2000).
[66] Ph. Wernet, D. Nordlund, U. Bergmann, M. Cavalleri, M. Odelius, H. Ogasawara, L. Å. Näslund, T. K. Hirsch, L. Ojamäe, P. Glatzel, L. G. M. Pettersson and A. Nilsson, Science **304,** 995 (2004).
[67] J. D. Smith, C. D. Cappa, K. R. Wilson, B. M. Messer, R. C. Cohen and R. J. Saykally, Science **306,** 851 (2004).
[68] J. R. Errington and P. G. Debenedetti, Nature **409,** 318 (2001).